Injection region propagation outside of geosynchronous orbit

E. Spanswick,[1,2] G. D. Reeves,[2] E. Donovan,[1] and R. H. W. Friedel[2]

Received 2 November 2009; revised 7 April 2010; accepted 21 April 2010; published 19 November 2010.

[1] Using radial alignments of the Polar and Geotail satellites with the Los Alamos National Laboratory (LANL) fleet of geosynchronous observations, we investigate the radial propagation of the dispersionless substorm injection region outside 6.6 R_E. We compare the delay between injection onset observed at geosynchronous orbit and a second spacecraft in the same meridian (within 1 hr of Magnetic Local Time (MLT)) but at a different radial distance. Our results are consistent with earlier studies showing predominantly Earthward propagation of the substorm injection region at or near geosynchronous orbit. However, observations with spacecraft located further down tail ($R > \sim 9\ R_E$) conclusively show that tailward propagation of the dispersionless injection region must also occur. A statistical study of events using 10 years of Polar, Geotail, and LANL observations shows that dispersionsless injections are most likely to initiate at radial distances of 6.6–9 R_E. Injections typically start at this location and expand radially inward toward geosynchronous orbit and outward into the midtail central plasma sheet. Implications of these results on injection region models are discussed.

Citation: Spanswick, E., G. D. Reeves, E. Donovan, and R. H. W. Friedel (2010), Injection region propagation outside of geosynchronous orbit, *J. Geophys. Res.*, *115*, A11214, doi:10.1029/2009JA015066.

1. Introduction

[2] Substorm injections are sudden and dramatic enhancements of several to hundreds of keV electrons and ions in the near-Earth plasma sheet in conjunction with a substorm expansion phase [*McIlwain*, 1974; *Moore et al.*, 1981; *Sauvaud and Winckler*, 1980]. We classify injections as being either dispersionless or dispersed. In a dispersionless injection, fluxes increase simultaneously across a range of energies, whereas in a dispersed injection, the flux increase is seen earlier at higher energies and later at lower energies. Dispersionless injections are characteristic of a flux increase that is observed within its source region, which, in turn, is referred to as the *dispersionless injection region* or simply the *injection region* [*McIlwain*, 1974]. Energetic particles have fairly rapid azimuthal (longitudinal) motion due to gradient-curvature drifts and therefore drift out of the injection region. Because these drifts are energy-dependent, substorm injections observed outside the injection region have a characteristic energy-dependent time delay referred to as *energy dispersion*. The characteristics of the particle flux as a function of energy and time can be used to determine the origin, extent, and propagation of the substorm injection.

[3] The physical shape of the injection region in the near-Earth plasma sheet was derived from early single-satellite observations. Injection statistics in the geosynchronous region led to the injection boundary model of *McIlwain* [1974]. In this model, the injection region appears at substorm onset with a well-defined Earthward boundary. At or tailward of the injection boundary, the signature is expected to be dispersionless with dispersed signatures seen in the MLT sectors outside the injection region. *Mauk and McIlwain* [1974] and *Lopez et al.* [1990] derived similar expressions for the location of the injection boundary as a function of local time and magnetic activity. Statistically, the boundary is observed to be radially closest to the Earth during higher magnetic activity (*Kp*) and at a specific local time. *Konradi et al.* [1975] extended the work of *Mauk and McIlwain* [1975], inferring a double spiral shape for the injection boundary with the closest radial distance to the Earth being in the midnight region. More recent work using CRRES data placed an outer boundary of the injection region from <5.2 R_E to >7.7 R_E (basically all L), and the inner boundary typically inside 6.3 R_E [*Friedel et al.*, 1996].

[4] The motion of the injection boundary during the substorm cycle was first described by *Moore et al.* [1981] in the convection surge model. *Moore et al.* viewed the injection boundary not as a stationary feature but rather as a front propagating Earthward over the course of the substorm cycle see left side of Figure 1 in *Reeves et al.* [1996]. In this model, the injection region first forms in the midtail and develops in such a way that it moves Earthward, increasing the particle energy through betatron and Fermi acceleration. A numerical simulation of this on the basis of earlier work by *Li et al.* [1998] and *Birn et al.* [1997a] was presented by *Sarris et al.* [2002]. They used an Earthward-propagating transient magnetic field pulse to represent the injection process. The strength of the pulse was sufficient to reverse the local magnetic field gradient at distances outside geosynchronous orbit, which, in turn, reduced or reversed a particle's azimuthal

[1]Department of Physics and Astronomy, University of Calgary, Calgary, Alberta, Canada.
[2]Los Alamos National Laboratory, Space Science & Application, Los Alamos, New Mexico, USA.

0148-0227/10/2009JA015066

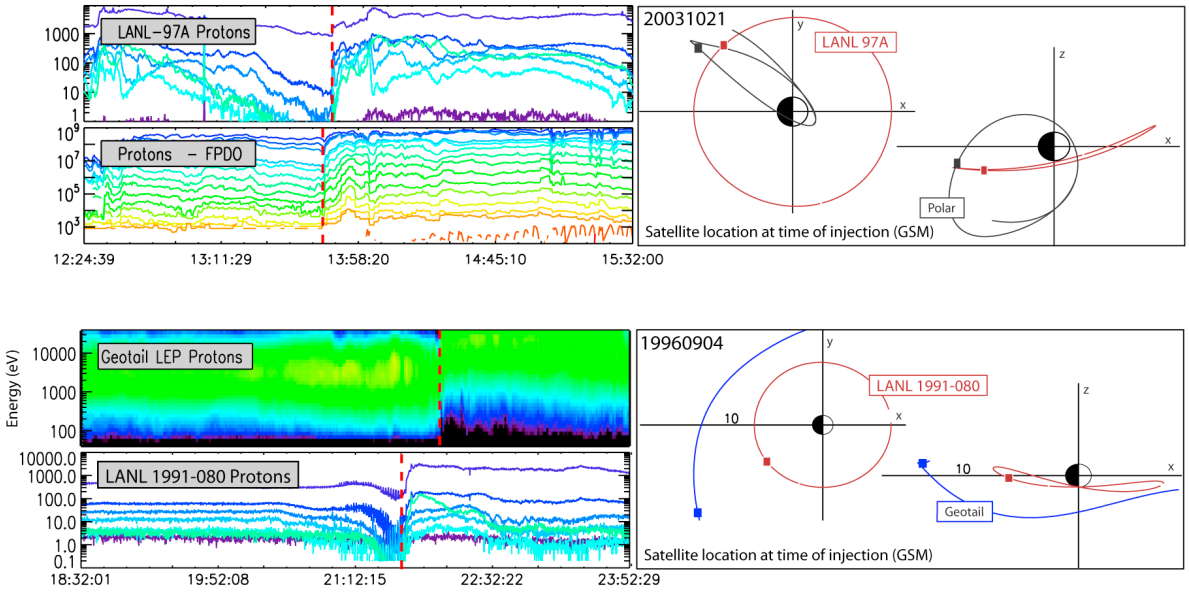

Figure 1. Example injection events from Polar/Geotail and Los Alamos National Laboratory (LANL). *Top*: Polar CEPPAD and LANL SOPA ion data (*bottom*: Geotail LEP and SOPA ion data) for an injection event in our data set. For Polar and LANL data, different energy channels are plotted in different colors, higher (lower) energy channels are plotted in red (blue). For Geotail LEP, energy is indicated in the *y*-axis and relative flux is indicated by the shading, black (orange) indicating a lower (higher) relative flux. Injections are indicated with red dashed lines. The satellite locations at the time of the observed injection are shown at the adjacent right.

drifts. This feature allowed the model to bring particles into the near-Earth plasma sheet without separation due to energy and species-dependent drifts. Particle energization in this model conserves the first two adiabatic invariants as a result of the Earthward motion of the injection region, and the particle source region for the injection is continuous across a wide range of radial distances (i.e., the pulse picks up and energizes particles along its path).

[5] A competing view of injection region evolution is one of localized onset near the inner edge of the plasma sheet, followed by Earthward motion and tailward expansion (see right side of Figure 1 in *Reeves et al.* [1996]). This sequence was first presented by *Lui et al.* [1988] and *Lopez et al.* [1990], who argued that the injection boundary represents the Earthward edge of the magnetotail undergoing current disruption during a substorm expansive phase. In this sense, the injection boundary is a physical boundary between the stable inner plasma sheet and the unstable (to current disruption) plasma sheet. The injection region forms on this boundary, where particles are locally accelerated, and then convects Earthward. *Birn et al.* [1997a] later showed that a convection surge model could also produce this macroscale evolution of the injection region (right side of Figure 1) without invoking localized acceleration. In that model, the region associated with the largest inductive electric field was located near the inner edge of the plasma sheet in response to flux pileup caused by the convection surge. The region of expanding inductive electric fields would be responsible for the energization of the particle population that composes the injection region and also its macroscale evolution. It should also be noted that all of the models described above were developed to explain the same signatures at geosynchronous orbit.

[6] Observations that enable investigations of the radial evolution of the injection region are few, because the majority of injection measurements come from in or around the geosynchronous region. Nevertheless, some progress along this line has been made. Using ATS-6 and SCATHA data, *Moore et al.* [1981] found that injections occur first at the satellite farthest from the Earth. *Thomsen et al.* [2001] found an azimuthal offset between ion and electron injection regions in the geosynchronous region, with electron injections offset eastward from their ion counterparts. This was initially predicted on the basis of observations by *Reeves et al.* [1991] and later incorporated in a model by *Birn et al.* [1997a]. Azimuthal separation of injections was attributed to the Earthward motion of the injection region subjecting the particle population to an increasing gradient curvature drift. These drifts must be large enough to shift the relative location of electrons and ions, but not so much as to cause dispersion within either population. Studies using data from closely separated radial alignments of CRESS and a Los Alamos National Laboratory (LANL) satellite have shown that the dispersionless injection typically evolves radially inward from the geosynchronous region, meaning that it starts somewhat farther out [*Reeves et al.*, 1996]. In that study, the authors found the average velocity of the injection region to be ~24 km/s Earthward from geosynchronous. These past results all suggest that the injection region forms (on average) somewhere outside geosynchronous orbit and evolves radially inward. However, these measurements (which are closely spaced with respect to the geosynchronous region) have not brought closure to the question, Where does the injection region form, and how does it evolve?

[7] Although difficult to interpret in a magnetospheric frame of reference, ionospheric measurements have shown

Table 1. List of Dispersionless Injection Used in This Study[a]

Date	Satellite ID	DI type	DI onset (UT)
23 Oct 1998	LANL-084	Electron	1608:39
	Polar		1611:54
29 Aug 2000	LANL-084	Electron	1835:07
	Polar		1834:43
1 Sep 2000	LANL-084	Electron	1905:27
	Polar		1904:07
29 Nov 2000	LANL-046	Electron	0639:26
	Polar		0637:38
27 Aug 2001	LANL-97 A	Electron	2011:51
	Polar		2010:10
31 Aug 2002	LANL-080	Electron	1134:41
	Polar		1141:28
3 Oct 2002	LANL-01 A	Electron	2227:14
	Polar		2230:26
25 Oct 2002	LANL-080	Proton	0802:53
	Polar		0810:41
10 Sep 2003	LANL-01 A	Proton	2328:51
	Polar		2324:30
20 Sep 2003	LANL-095	Electron	0203:22
	Polar		0206:49
21 Sep 2003	LANL-97 A	Proton	1649:51
	Polar		1645:19
23 Sep 2003	LANL-01 A	Proton	2344:02
	Polar		2343:01
24 Sep 2003	LANL-02 A	Electron	1904:53
	Polar		1902:39
21 Oct 2003	LANL-97 A	Proton	1349:26
	Polar		1346:10
24 Oct 2003	LANL-02 A	Proton	1533:03
	Polar		1528:09
12 Nov 2003	LANL-01 A	Proton	1852:00
	Polar		1850:33
26 Oct 1997	LANL-97 A	Electron	2041:30
	Geotail		2047:25
22 Sep 1998	LANL-97 A	Electron	1929:51
	Geotail		1932:26
21 Sep 1999	LANL-046	Electron	1319:11
	Geotail		1324:57
6 May 2000	LANL-080	Electron	2329:21
	Geotail		2323:03
29 Jul 2002	LANL-095	Electron	0355:32
	Geotail		0354:59
27 Dec 2003	LANL-97 A	Electron	2126:49
	Geotail		2117:08

[a]For Each Event, the Pair of Satellites is Identified Along with the Corresponding Dispersionless Injection (DI) Type and the Onset of Dispersionless Injection (DI) at Each Satellite.

some promise in this area. *Spanswick et al.* [2007] showed that it is possible to identify dispersionless electron injections using ground-based riometer data. In that study, the authors noted that the radial evolution of the ionospheric footprint of the injection region can be followed using a wide array of riometers. They showed that dispersionless injections are first seen at a specific latitude (typically corresponding to L $\approx$ 8) and then expand equatorward and poleward. Although it is unlikely, if not impossible, to infer precisely the magnetospheric location from ionospheric measurements, at the very least these results imply that the injection region has well-defined Earthward and tailward boundaries.

[8] The goal of this study is to look for in situ observational support for either an outside-in or an inside-out scenario. We used the same methodology as *Reeves et al.*, [1996] but applied to the region outside geosynchronous orbit. Although this study does not identify the physical mechanism responsible for the injection region, it does provide in situ observational constraints on injection models and give magnetospheric context to the statistical results from ionospheric measurements. We use LANL particle measurements from geosynchronous orbit in conjunction with measurements from Polar and Geotail to resolve the radial propagation of the injection region outside geosynchronous orbit. Specifically, we use two-satellite radial alignments to determine the delay between the start of the injection seen at one satellite relative to its beginning at the other. The radial separation of the two satellites is larger than those in the previous studies of radial evolution of injection, which only allowed the determination that most injections evolve Earthward in the geosynchronous region [*Moore et al.*, 1981; *Friedel et al.*, 1996]. Our objectives are to determine whether there is an identifiable radial distance for the beginning of substorm injections and to confirm or refute the presence of a tailward evolving outer radial boundary of the injection region.

2. Data

[9] We use data from the SOPA detector on board the LANL network of geosynchronous satellites [*Belian et al.*, 1992]. SOPA provides electron and ion measurements at a temporal cadence of ~10 sec in the energy range 50 keV to 1.5 MeV for electrons and 50 keV to 7.7 MeV for protons. From 1996 to 2006, the Polar orbit precessed and sampled the plasma sheet from L ~4 to ~10. The CEPPAD detector onboard Polar records fluxes of both ions and electrons from the ranges 20 keV to ~1 MeV [*Blake et al.*, 1995]. We also use data from the Geotail Low Energy Plasma detector (LEP), which provides electron and ion measurements from 32 eV/q to 39 keV/q every 12 sec [*Mukai et al.*, 1994]. In this study, we used omnidirectional data (i.e., not pitch angle resolved) from all three satellites.

3. Observations

[10] We searched the ephemeris data from Polar (1996–2006) for periods in which (1) Polar was within 15° latitude of the geographic equatorial plane, (2) Polar was within ±5 hr of midnight magnetic local time (MLT), and (3) Polar was within ±1 hr of MLT of a LANL spacecraft. Within these candidate time periods (in total there were 3500), we manually searched for injection events that could be seen in both Polar and the appropriate LANL spacecraft. We selected both ion and electron injection events fitting the dispersionless criteria of *Birn et al.* [1997b], which requires a flux increase in more than two energy channels in <2 min. We also made an effort to exclude lobe to plasma sheet transitions (which have a similar signature in the high-energy particle data) by looking at the CEPPAD electrons (50 keV +) prior to the injection observation. In general, the lobe is devoid of high-energy electrons [*Baumjohann et al.*, 1988], so their presence during the growth phase prior to the observed injection can be used to differentiate between local plasma sheet thickening (and/or motion of the satellite) and a dispersionless injection. In total, we found 17 events

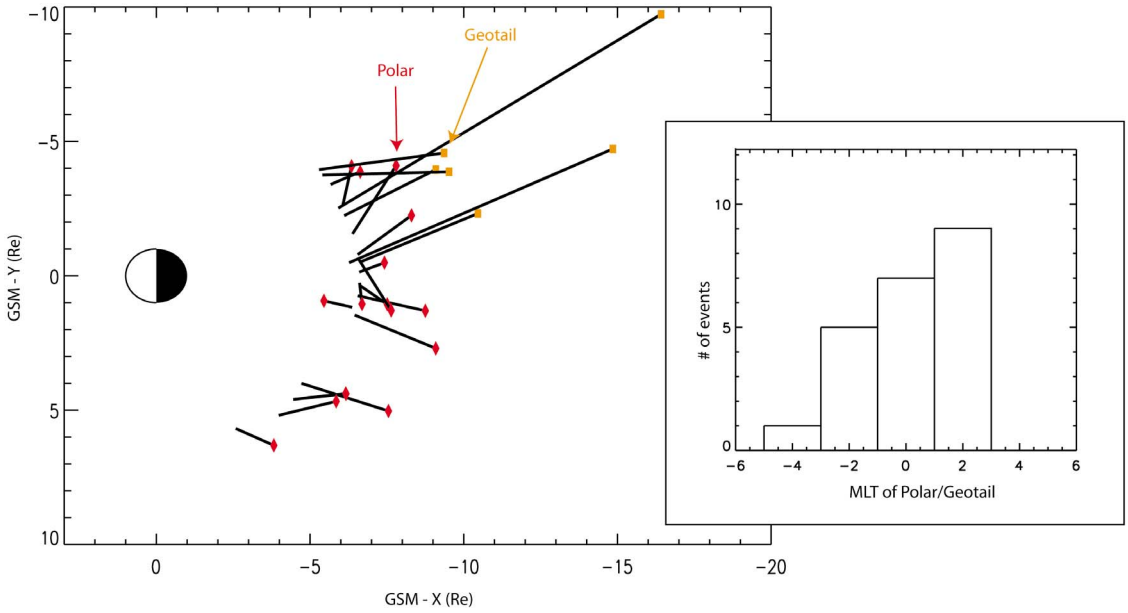

Figure 2. GSM-XY locations of the satellites used for each event. Events are shown as lines that connect the location of Polar or Geotail (shown as red diamonds or yellow squares) to a location of the appropriate LANL spacecraft in geosynchronous orbit. The MLT distribution of events is shown in the bottom right.

that fit our criteria, an example of which is presented in the top of Figure 1. This relatively small number of events is understandable given the need for a serendipitous alignment of the satellites, the orbit of Polar (which cuts through the plasma sheet), the small MLT window, the requirement that the Polar not transition in the lobe, and the observation of an injection at both satellites.

[11] We preformed the same ephemeris search for the Geotail satellite with an additional criteria that Geotail have $X_{GSM} > -30\ R_E$. This produced approximately 300 candidate time periods. Because we used LEP data in this study, the lobe to plasma sheet transitions are easily removed from our dataset. Using the *Eastman et al.* [1998] guidelines for identifying the plasma sheet, we only use events in which Geotail was in the plasma sheet during the growth phase prior to the injection. Because the Geotail apogee is quite deep in the magnetotail, it was in general more difficult to find events in which it remained in the plasma sheet during the growth phase. This preferentially gave us events in the near-Earth region ($X \sim -12\ R_E$), where the plasma sheet is thicker and Geotail is less likely to transition to the lobe in the growth phase. An example event from Geotail is shown in the bottom of Figure 1. Table 1 is a complete list of all events used in this study, including satellite names and injection onset times. The GSM-XY locations of all events used in this study are shown in Figure 2. The locations of Polar and Geotail are indicated with red diamonds and orange squares, respectively. Each event is indicated with a line connecting the location of Polar or Geotail to the location of the LANL spacecraft. The MLT distribution of events is also shown in the lower right inset in Figure 2.

[12] In this study, we reference all timing to geosynchronous orbit (i.e., we report the injection delay time relative to the injection observed by LANL with positive delay times indicating observation times earlier than LANL's) and illustrate our examples with constant velocities (straight lines). Figure 3 shows the two possible scenarios in this study: an injection observed before LANL (Type A) and an injection observed after LANL (Type B). Injection observations are indicated with stars. The range of possible onset times and locations that are consistent with the observed time differences are shown with shading. Two examples of possible onset times and locations for each type (A and B) are shown with yellow dots. Radial propagation is shown with arrows for either Earthward (red) or tailward (blue) propagation. The first event type (Type A) shown at the left of Figure 3, has a positive delay time relative to geosynchronous orbit, meaning that at some distance R ($R > 6.6\ R_E$), the satellite observed an injection earlier than the injection was seen at geosynchronous. In this case, it is possible that the injection region (shown as yellow dots) originated tailward of Polar/Geotail and moved toward geosynchronous (red dotted line) or that the injection originated between Polar/Geotail and geosynchronous and propagated both Earthward and tailward (solid lines). If, as we assume here, the Earthward and tailward velocities are equal, then, for this scenario, the onset region would have to be closer to Polar/Geotail than to geosynchronous orbit. If we relax that assumption and allow different (average) Earthward and tailward velocities, then the onset could lay anywhere tailward of geosynchronous orbit. There are, in fact, an infinite number of possibilities to connect the signatures seen at two satellites, and we cannot unambiguously differentiate between any of them with just two point measurements. Because our interpretation is made on the basis of purely radial motion, we can only argue that the injection region could

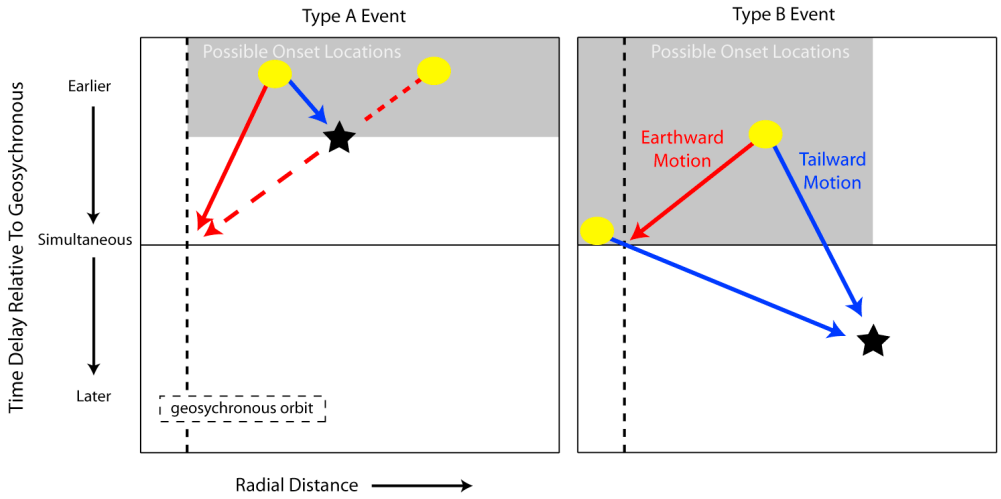

Figure 3. The expected time delay between observations at a radial distance R and geosynchronous observations as a function of the nongeosynchronous satellites radial distance. An injection observation (at a location R) is indicated with a star. The possible injection onset locations are shown as yellow dots, which are connected to the observations using red (Earthward propagation) and blue (tailward propagation) lines. Event types A and B correspond to two possibilities, seeing an injection prior to A and after B geosynchronous observations of the same injection event. Figure 3 is discussed in the Observations section.

not have formed inside of geosynchronous orbit for this class of events.

[13] The second possibility is a dispersionless injection observed at geosynchronous orbit first and then some time later at Polar/Geotail. (Possible onset locations for Type B events shown in the right of Figure 3.) For events for which the injection was seen first at geosynchronous orbit, the argument is similar to but opposite to that for Type A events. Again, the injection onset could begin anywhere Earthward of geosynchronous orbit or anywhere between the two satellites but could not have originated tailward of Polar/Geotail.

4. Results

[14] Although for any given event the relative injection observation times between Polar/Geotail and LANL cannot unambiguously determine the injection onset location, the statistical ensemble gives us more hints as to the likely average location. Figure 4 shows the observed delay times between injection onset seen at Polar/Geotail and LANL as a function of the geocentric radial distance of Polar/Geotail when the satellites were within 1 hr of MLT. This plot is in the same format as Figure 3: Geotail-LANL and Polar-LANL events are shown with black and blue dots, respectively. Using all 10 years of Polar/Geotail-LANL radial conjunctions, Figure 4 shows that there are clear trends in data from which we can infer some general properties of the spatiotemporal evolution of the injection region.

[15] We observe both positive and negative delay times (again, positive delay times indicate Polar/Geotail injections that are earlier than the injection observed at LANL). The negative delay times seen by Polar and Geotail were only observed outside ~9 R_E and highlighted with a blue swath. In these events, the injection region must have formed somewhere Earthward of Polar/Geotail. This confirms that, at least in those cases, there was an outer radial boundary to the injection region which evolved tailward.

[16] Seven of the nine events outside 9 R_E had negative delay times, suggesting that the injection region on average forms inside of that boundary. Inside 9 R_E we typically observed positive delay times (highlighted in Figure 4 with a red swath). In these events, the injection region must have formed outside geosynchronous orbit. We only found one event in our study in which Polar observed an injection inside geosynchronous. This event, with a negative delay time, is also consistent with Earthward propagation as seen in earlier studies that included many more events [e. g., *Reeves et al.*, 1996]. These two groups (negative and positive delay times) show conclusively that both Earthward and tailward propagation of the injection region can and does occur. Furthermore, seen as an ensemble, the radial dependence of the time delays strongly suggests that the location where the injection region forms is typically between 6.7 (e.g., geosynchronous) and 9 R_E.

5. Discussion

[17] The objectives of this study were to determine whether there is an identifiable radial distance for the beginning of substorm injections and to confirm or refute the presence of a tailward evolving outer radial boundary of the injection region suggested by ionospheric measurements. We surveyed data from Polar and Geotail and identified events where either Polar or Geotail was within 1 hr of MLT of a LANL spacecraft and where a dispersionless injection was observed by both the LANL spacecraft and the more distant satellite. We interpret the delay time between geosynchronous orbit and distances downtail as a consequence of the radial evolution of the injection region. Although each individual event tells us little about the behavior of the

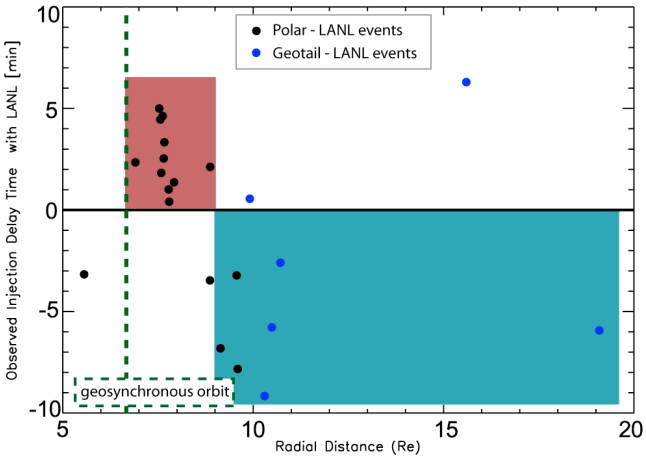

Figure 4. Observed delay times between Polar/Geotail and LANL as a function of Polar/Geotail radial distance. Polar-LANL injection events are indicated with black dots, and Geotail-LANL with blue dots. Figure 4 is discussed in the Results section.

injection region, the combination of all events gives us a statistical picture of the radial evolution of the injection region.

[18] In our survey, Polar and Geotail measurements from outside 9 R_E show irrefutable evidence that the injection region formed inside that distance and propagated outward toward Polar/Geotail. Furthermore, in our survey, results from events where the outer satellite was inside 9 R_E are consistent with the injection region having formed outside geosynchronous distance. Together these results imply a radially localized region (6.7–9 R_E) within which, on average, the injection region forms. These results are consistent with previous work that suggests the onset of injection is outside geosynchronous orbit and moves inward across that L shell.

[19] The existence of negative delay time events (geosynchronous observes an injection prior to the satellite further downtail) implies that in at least some cases, there must be a tailward boundary to the injection region and this boundary is propagating downtail. This result is consistent with the interpretation of the aforementioned ground-based auroral observations [*Spanswick et al.*, 2007], which placed dynamic Earthward and tailward boundaries on the injection region. This also implies that the ionospheric projection of the injection region, in some sense, reflects actual propagation in the magnetosphere, although to what degree we cannot speculate.

[20] Although it does not change the overall picture presented here, we found a large range (from 24 sec to 5 min) of delay times between injection observed at geosynchronous and at the outer satellite, when the outer spacecraft was between 7 and 9 R_E (see Figure 4). This may indicate angled injection fronts which are not accounted for in our purely radial interpretation of the delay times or simply the expected variability in the Earthward and tailward flow speeds.

[21] Our results do not validate a specific model for injection region generation. We are however, able to comment on aspects of certain models affected by our results. The average radial onset location for the injection region presented here has implications for convection surge type models where particle energization is accomplished via transport, moving particles from a region of lower to one of higher magnetic field strength [*Sarris et al.*, 2002; *Sarris and Li*, 2005]. In this type of transport; where the pulse initiates, how it moves (speed and deceleration), the local source population, and the magnetic field configuration along its path completely determine the location and energy content of the injection region. *Sarris et al.* [2002] demonstrated that a slower moving, faster-decelerating pulse is more effective in energizing and transporting particles. *Sarris and Li* [2005] further suggested that if the physical counterpart of the pulse is a magnetospheric fast flow, it would brake in the inner plasma sheet as a consequence of the balance between an Earthward magnetic tension force and a tailward pressure force, $-\nabla P_T$, [*Shiokawa et al.*, 1997], where the total pressure, P_T is given by $P_T = B^2/2\mu_0 + n_i kT_i$, where B is the magnetic field strength, k is the Boltzmann constant, T_i is the ion temperature and n_i is the ion density. This implies that a sharp increase in either ion density and/or magnetic field strength would cause a sudden deceleration of the pulse and an injection at that location. Because our results indicate the injection region initiates in the region between 6.7 and 9 R_E, the majority of the energy must come from this region. That is, the injection must first appear here. It cannot be a slow rise in energy as the particle population is transported Earthward from the midtail. For a purely transport driven model of the injection region to be consistent with the results presented here, the boundary of flux pile up must be quite sharp and, on average, occur in the region of 6.7–9 R_E in the late growth phase. In this type of model, the tailward propagation of the pileup also accounts for the tailward propagation of the injection region [*Birn et al.*, 1997a].

[22] At face value, the propagation of the injection region reported here is consistent with the predictions of the current disruption (CD) model. Our results, however, put important new constraints on the location at which CD initiates and how CD could produce the observed properties of substorm injections. The break point between positive and negative delay times suggests that the boundary between the stable (with respect to CD) inner plasma sheet and the unstable outer plasma sheet typically lies in the vicinity of ~8–9 R_E. This is consistent with statistical studies which place the CD region on average at distances of <15 R_E [*Ohtani et al.*, 1992]. This range is also quite close to the observed radial break point (X = ~11 R_e) between two classes of Earthward plasma flows reported by *Shue et al.* [2008]. In that study, the authors ascribed the two classes of flows to CD-driven flows (Earthward of ~11 R_e) and reconnection-driven flows (tailward of ~11 R_e). The Earthward propagation of the injection region from its initial onset location is somewhat harder to reconcile with the CD model. For distances <9 R_E, our results suggest a dominance of Earthward propagation (although some tailward propagation in that region is also possible as sketched in Figure 3). Earlier work by *Ohtani* [1998], using observations of dipolarization in the near-geosynchronous region, suggested that the region of disrupted current does indeed propagate Earthward. In this paradigm, the observed dipolarization is a remote effect from the Earthward propagating CD region and the injection boundary is located tail-

ward on the leading edge of the CD region. Also, the inward motion of the CD region is ascribed to field line dipolarization.

[23] Our results provide new information and raise new questions about the initiation and propagation of the substorm injection region that need to be taken into account in either the CD and Near-Earth Neutral Line (NENL) paradigms within which most substorm studies are framed [*Lui*, 1991; *Baker et al.*, 1996]. We have found that, statistically, there is a fairly distinct location in the tail at a distance of ~9 R_E, where injection region propagation switches from predominantly Earthward to predominantly tailward. Our results show conclusively that there must be both Earthward and tailward propagation of the dispersionless substorm injection region and strongly suggest that individual events have both (which could be verified in three-satellite studies if the right alignments can be found). In the context of the NENL model, tailward propagation provides interesting constraints on where and how flux pileup must occur and what the growth phase radial gradient in the plasma sheet must be to explain the observed particle energization. In the CD paradigm, it is the Earthward propagation that requires further investigation and, in particular, the location of instability onset relative to the transition between dipole-like and taillike field lines.

[24] We plan to follow this paper with a more detailed study on the characteristics of the individual events, for example, the associated electric and magnetic field measurements from Polar/Geotail and the presence of inductive electric fields. It is also possible to expand this study to include data from the five THEMIS spacecraft and investigate the relative occurrence rate of dispersionless injections at different radial distances during known substorm injection events. For example, how likely is it to observe an injection at $X = -12$ R_e when an injection is observed at $X = -10$ R_e? This would place further constraints on the overall radial extent of the injection region.

[25] **Acknowledgments.** We thank T. Nagai and T. Mukai for making the Geotail LEP and MFI data available through the CDAWeb data facility operated and maintained by the NSSDC. The work of ES and ED is supported by the Natural Sciences and Engineering Research Council (Canada), the Alberta Ingenuity Fund, and the Canadian Space Agency.

[26] M. Fujimoto thanks A. Lui and T. Sarris for their assistance in evaluating this paper.

References

Baker, D., T. Pulkkinen, V. Angelopoulos, W. Baumjohann, and R. McPherron (1996), Neutral line model of substorms: Past results and present view, *J. Geophys. Res.*, *101*(A6), 12,975–13,010, doi:10.1029/95JA03753.

Baumjohann, W., G. Paschmann, N. Sckopke, C. A. Cattell, and C. W. Carlson (1988), Average ion moments in the plasma sheet boundary layer, *J. Geophys. Res.*, *93*(A10), 11,507–11,520, doi:10.1029/JA093iA10p11507.

Belian, R. D., G. R. Gisler, T. Cayton, and R. Christensen (1992), High-Z energetic particles at geosynchronous orbit during the great solar proton event of October 1989, *J. Geophys. Res.*, *97*(A11), 16,897–16,906, doi:10.1029/92JA01139.

Blake, J. B., et al. (1995), CEPPAD: Comprehensive energetic particle and pitch angle distribution experiment on POLAR, *Space Sci. Rev.*, *71*, 531–562.

Birn, J., M. Thomsen, J. Borovsky, G. Reeves, D. McComas, R. Belian, and M. Hesse (1997a), Substorm ion injections: Geosynchronous observations and test particle orbits in three-dimensional dynamic MHD fields, *J. Geophys. Res.*, *102*(A2), 2325–2341, doi:10.1029/96JA03032.

Birn, J., M. F. Thomsen, J. E. Borovsky, G. D. Reeves, D. J. McComas, and R. D. Belian (1997b), Characteristic plasma properties during dispersionless substorm injections at geosynchronous orbit, *J. Geophys. Res.*, *102*(A2), 2309–2324.

Eastman, T. E., et al. (1998), Magnetospheric plasma regimes identified using Geotail measurements 1. Regime identification and distant tail variability, *J. Geophys. Res.*, *103*(A10), 23,503–23,520, doi:10.1029/98JA01915.

Friedel, R. H. W., A. Korth, and G. Kremser (1996), Substorm onsets observed by CRRES: Determination of energetic particle source regions, *J. Geophys. Res.*, *101*(A6), 13,137–13,154, doi:10.1029/96JA00399.

Konradi, A., C. L. Semar, and T. A. Fritz (1975), Substorm-injected protons and electrons and the injection boundary model, *J. Geophys. Res.*, *80*(4), 543–552, doi:10.1029/JA080i004p00543.

Li, X., D. N. Baker, M. Temerin, G. D. Reeves, and R. D. Belian (1998), Simulation of dispersionless injection and drift echos of energetic electrons associated with substroms, *Geophys. Res. Lett.*, *25*(20), 3763–3766, doi:10.1029/1998GL900001.

Lopez, R. E., D. G. Sibeck, R. W. McEntire, and S. M. Krimigis (1990), The energetic ion substorm injection boundary, *J. Geophys. Res.*, *95*(A1), 109–117, doi:10.1029/JA095iA01p00109.

Lui, A. (1991), A synthesis of magnetospheric substorm models, *J. Geophys. Res.*, *96*(A2), 1849–1856, doi:10.1029/90JA02430.

Lui, A. T. Y., and S. M. Krimigis (1988), Behavior of energetic ions of different ionic species during substorm injections, *Eos Trans.*, *69*, 1382.

Mauk, B. H, and C. E. McIlwain (1974), Correlation of *Kp* with the substorm injected plasma boundary, *J. Geophys. Res.*, *79*(22), 3193–3196, doi:10.1029/JA079i022p03193.

McIlwain, C. E. (1974), Substorm injection boundaries, in *Magnetospheric Physics*, edited by B. M. McCormac, p. 143, D. Reidel, Norwell, MA.

Moore, T. E., R. L. Arnoldy, J. Feynman, and D. A. Hardy (1981), Propagating substorm injection fronts, *J. Geophys. Res.*, *86*(A8), 6713–6726, doi:10.1029/JA086iA08p06713.

Mukai, T., S. Machida, Y. Saito, M. Hirahara, T. Terasawa, N. Kaya, T. Obara, M. Ejiri, and A. Nishida (1994), The low energy particle (LEP) experiment onboard the Geotail satellite, *J. Geomag. Geoelectr.*, *46*, 669–692.

Ohtani, S. (1998), Earthward expansion of the tail current disruption: Dual-satellite study, *J. Geophys. Res.*, *103*(A4), 6815–6825, doi:10.1029/98JA00013.

Ohtani, S., S. Kokubun, and C. T. Russell (1992), Radial expansion of the tail current disruption during substorms: A new approach to the substorm onset region, *J. Geophys. Res.*, *97*(A3), 3129–3136, doi:10.1029/91JA02470.

Reeves, G. D., R. D. Belian, and T. E. Fritz (1991), Numerical tracing of energetic particle drifts in a model magnetosphere, *J. Geophys. Res.*, *96*(A8), 13,997–14,008, doi:10.1029/91JA01161.

Reeves, G. D., M. G. Henderson, P. S. McLachlan, R. D. Belian, R. H. W. Friedel, and A. Korth (1996), Radial propagation of substorm injections, in *Proceedings of the Third International Conference on Substorms*, Eur. Space Agency Spec. Publ., ESA SP-389, 579.

Sarris, T. E., and X. Li (2005), Evolution of the dispersionless injection boundary associated with substorms, *Ann. Geophys.*, *23*, 877–884.

Sarris, T. E., X. Li, N. Tsaggas, and N. Paschalidis (2002), Modeling energetic particle injections in dynamic pulse fields with varying propagation speeds, *J. Geophys. Res.*, *107*(A3), 1033, doi:10.1029/2001JA900166.

Sauvaud, J.-A., and J. R. Winckler (1980), Dynamics of plasma, energetic particles and fields near synchronous orbit in the nighttime sector during magnetospheric substorms, *J. Geophys. Res.*, *85*(A5), 2043–2056, doi:10.1029/JA085iA05p02043.

Shiokawa, K., W. Baumjohann, and G. Haerendel (1997), Braking of high-speed flows in the near-Earth tail, *Geophys. Res. Lett.*, *24*(10), 1179–1182, doi:10.1029/97GL01062.

Shue, J.-H., A. Ieda, A. T. Y. Lui, G. K. Parks, T. Mukai, and S. Ohtani (2008), Two classes of earthward fast flows in the plasma sheet, *J. Geophys. Res.*, *113*, A02205, doi:10.1029/2007JA012456.

Spanswick, E., E. Donovan, R. Friedel, and A. Korth (2007), Ground based identification of dispersionless electron injections, *Geophys. Res. Lett.*, *34*, L03101, doi:10.1029/2006GL028329.

Thomsen, M. F., J. Birn, J. E. Borovsky, K. Morzinski, D. J. McComas, and G. D. Reeves (2001), Two-satellite observations of substorm injections at geosynchronous orbit, *J. Geophys. Res.*, *106*(A5), 8405–8416, doi:10.1029/2000JA000080.

E. Donovan and E. Spanswick, Department of Physics and Astronomy, University of Calgary, 2500 University Drive N.W., Calgary, AB T2 N 1N4, Canada. (elspansw@lanl.gov)

R. H. W. Friedel and G. D. Reeves, Los Alamos National Laboratory, Space Science & Application, ISR-1 MS-D466, Los Alamos, NM 87545, USA.